atoms

MDPI

Article

# Cobalt-Hydrogen Atomic and Ionic Collisional Data

**Svetlana A. Yakovleva [1,*], Andrey K. Belyaev [1,*] and Maria Bergemann [2,*]**

[1] Department of Theoretical Physics and Astronomy, Herzen University, 191186 St. Petersburg, Russia
[2] Max-Planck Institute for Astronomy, 69117 Heidelberg, Germany
* Correspondence: sayakovleva@herzen.spb.ru (S.A.Y.); andrey.k.belyaev@gmail.com (A.K.B.); bergemann@mpia-hd.mpg.de (M.B.)

Received: 22 June 2020; Accepted: 8 July 2020; Published: 13 July 2020


**Abstract:** Rate coefficients for inelastic processes in low-energy Co + H, $Co^+ + H^-$, $Co^+ + H$, and $Co^{2+} + H^-$ collisions are estimated using the quantum simplified model. Considerations include 44 triplet and 55 quintet molecular states of CoH, as well as 91 molecular states of $CoH^+$. The estimations provide the rate coefficients for the 4862 partial processes (mutual neutralization, ion-pair formation, excitation, and de-excitation) in the neutral CoH system, and for the 8,190 partial processes in the ionized $CoH^+$ system, 13,052 processes in total. At $T = 6000$ K, the rate coefficients with the largest values around $6 \times 10^{-8}$ $cm^3s^{-1}$ correspond to the mutual neutralization processes into the $Co(e^2F) + H$ and $Co^+(g^5F) + H$ final channels in the neutral and ionized systems, respectively. Among the excitation and de-excitation processes in Co + H and in $Co^+ + H$ collisions, at $T = 6000$ K, the largest rate coefficients have values around $7 \times 10^{-9}$ $cm^3s^{-1}$ and correspond to the processes $Co(y^2S^\circ) + H \rightarrow Co(e^2F; v^4D^\circ) + H$ and $Co^+(h^3P) + H \rightarrow Co^+(g^3P; g^5P; g^5F) + H$, respectively. The calculations single out inelastic processes important for non-local thermodynamic equilibrium (NLTE) modelling of Co I and Co II spectra in stellar atmospheres. The test NLTE calculations are carried out, and it is found that the new collision rates have a strong effect on the line formation and NLTE abundance corrections.

**Keywords:** atomic collisional data; atomic inelastic processes; rate coefficients; stars; atmospheres

## 1. Introduction

Determination of the stellar absolute and relative abundances for different chemical elements is one of the fundamental problems in modern astrophysics, see, e.g., reviews [1,2] and references therein, for example, for understanding the Big Bang, stellar evolution, and microscopic processes in stars. As is known, Local Thermodynamic Equilibrium (LTE) modelings of stellar spectra provide not sufficiently accurate results, and non-Local Thermodynamic Equilibrium (NLTE) modelings are used for more accurate treatments [1,2]. NLTE modeling requires detailed and complete information about radiative and non-radiative inelastic physical processes, i.e., the mutual neutralization, ion-pair formation, excitation, and de-excitation processes in atom-atom and positive-negative-ions collisions. The important processes for these purposes are those taken place in collisions of heavy particles with hydrogen atoms and anions. The lack of reliable data on H-collisional data, i.e., inelastic processes in collisions of atoms and positive ions of a treated chemical element with hydrogen atoms and negative ions, brings the main uncertainty in NLTE modelings due to the highest abundance of hydrogen in the Universe.

It is important to know these data not for one collision process, but for hundreds, thousands, and even millions processes. Experiments, especially, for low-energy neutral-particle collisions are very seldom, so the main source of collisional data is theoretical calculations. Full quantum studies based on accurate quantum chemical calculations are rather time-consuming, and therefore, were performed

for a few low-energy H-collisions only: Na + H and $Na^+ + H^-$ [3,4], Li + H and $Li^+ + H^-$ [5–7], Mg + H and $Mg^+ + H^-$ [8,9], He + H [10], Ca + H and $Ca^+ + H^-$ [11,12], as well as $H^- + H^+$ [13,14], see also references therein. For this reason, during many years the so-called Drawin formula [15–18] has been used for estimating atomic collision data, until it was recognized [19] that the Drawin formula is not reliable: It does not have a correct physical background, it overestimates rate coefficients by up to several orders of magnitude for some processes, while underestimates up to several orders of magnitude for some other processes. A demand in reliable H-collision data from the stellar atmosphere NLTE modeling community is still large, in particular, to replace Drawin's data. Thus, the motivation of the present paper is to provide data for inelastic processes: Mutual neutralization, ion-pair formation, excitation and de-excitation, in collisions Co + H, $Co^+ + H^-$, $Co^+$ + H, $Co^{2+} + H^-$. Finally, the present paper provides these data for 13,052 partial inelastic processes in cobalt-hydrogen collisions in the temperature range 1000–10,000 K.

Cobalt is one of the key Fe-group elements that is commonly used to trace explosive nucleosynthesis in core-collapse and SN Ia [20]. In the spectra of FGK stars, Co is represented by several strong lines of neutral Co I, which offer a powerful diagnostic of Co abundances across a wide metallicity range [21,22].

The astrophysical origin of Co is still poorly understood, as the models of Galactic chemical evolution fail to explain the abundances of Co relative to Fe in the disk and in the halo (e.g., Andrews et al. [23], Côté et al. [24]). This mismatch is commonly attributed to the uncertainties of core-collapse and SN I models [20]. In terms of nucleosynthesis, Co is produced in complete Si-burning and $\alpha$-rich freeze-out during explosion. Co is a neutron-rich element and its production is expected to be sensitive to the explosion entropy and to the neutron excess during explosion, hence, to the metallicity of progenitors.

Observational constraints on the chemical evolution and nucleosynthesis of Co in the Galaxy are still limited by the incomplete understanding of line formation of Co I in FGK-type spectra. The classical models, which employ 1D hydrostatic models and local thermodynamic equilibrium (LTE), suggest that the [Co/Fe] ratio is essentially constant around solar metallicities, but only mildly increases towards lower [Fe/H] in the local Galactic neighbourhood (e.g., Battistini and Bensby [22], Lomaeva et al. [25]). In dSph galaxies, Co/Fe ratios appears to be slightly super-solar [26,27]. This suggests that Co is slightly over-produced compared to Fe in core-collapse supernovae, but closely follows Fe production in SN Ia.

Yet, recent efforts to include departures from LTE in the framework of solving statistical equilibrium, suggest that 1D LTE massively under-estimates the abundance of Co in FKG stars, with far-reaching implications for the astrophysical interpretation of the abundance trends in the Galaxy.

In this work, we re-assess the quality of the model used to perform non-local thermodynamic equilibrium (NLTE) calculations of Co in late-type stars. For this, we carry out detailed quantum-mechanical calculations of inelastic processes in collisions with hydrogen, which have represented a key uncertainty in our earlier study. We then employ the new H collision rates to updated our model atom and to recompute the statistical equilibrium for several model atmospheres across a range of metallicities. We compare our results with our previous predictions and quantify the importance of quantum H-collision data in the NLTE modelling of Co lines.

## 2. Inelastic Collisions with Hydrogen

To estimate the rate coefficients for inelastic processes in collisions of cobalt atoms and positive ions with hydrogen atoms and negative ions, i.e., in Co + H, $Co^+ + H^-$, $Co^+$ + H, $Co^{2+} + H^-$ collisions, the quantum simplified model [28,29] is implied. The point is that the reaction mechanisms of the inelastic H-collision processes have been thoroughly treated in the fully quantum studies cited above and it has been demonstrated the importance of the long-range ionic-covalent avoided crossing mechanism leading naturally to charge transfer processes (mutual neutralization and ion-pair production), in addition to excitation and de-excitation processes, although other mechanisms have been considered

as well. Because of the importance of the long-range ionic-covalent mechanism, the simplified model has been developed [28,29]. This model may be particularly useful in cases when suitable quantum chemical data are not available.

The simplified model is based on the semi-empirical ionic-covalent interactions [30] determining a long-range electronic structure of a collisional system [31] followed a nonadiabatic nuclear dynamical study by means of the Landau-Zener model [32–34] with the adiabatic-potential-based formula [35] for nonadiabatic transition probabilities. The simplified model shows that rate coefficients for mutual neutralization and ion-pair formation processes depend on a single energy, a binding energy of a covalent state, while rates for excitation and de-excitation processes depend on two energies, binding energies of an initial and a final covalent states. The dependence of reduced rate coefficients on a binding energy/energies is tabulated by Belyaev and Yakovleva [28,29], so in order to get a value of an inelastic-process rate coefficient one does not need to calculate anything, it is sufficient to know a binding energy/energies for a particular partial process, to determine a statistical weight and finally to get a rate coefficient from the tabulated dependence and a simple formula. Please note that the simplified model has been developed for a ground ionic molecular state. If an excited ionic state should be treated, see below, then another binding energy for an ionic state should be taken and reduced rates should be recalculated appropriately as it is done below. Finally, the simplified model allows one to estimate rate coefficients for inelastic H-collision processes from known atomic/ionic energy levels (which determine binding energies) without any additional calculations.

By comparison with full quantum calculations, it was shown that the simplified model provides reliable rate coefficients with large and intermediate values and reasonable estimates for low-valued rates. The comparison was done for collisions of hydrogen with sodium [3,4], lithium [5,6], and magnesium [8,9]. The simplified model was successfully applied to several collisional systems, including iron-hydrogen atomic collisions [36] and iron-hydrogen ionic collisions [37].

In case of CoH, two ionic molecular channels are included into consideration. The ground ionic state $Co^+(3d^8\,{}^3F) + H^-$ has four molecular symmetries $^3\Sigma^-$, $^3\Pi$, $^3\Delta$ and $^3\Phi$. The first-excited ionic molecular state $Co^+(3d^7 4s\,{}^5F) + H^-$ is around 0.515 eV higher than the ground ionic state and provides another multiplicity, it has $^5\Sigma^-$, $^5\Pi$, $^5\Delta$ and $^5\Phi$ molecular symmetries. Tables A1 and A2 contain 44 triplet and 55 quintet molecular states, respectively. Within the simplified model, only rate coefficients due to one-electron transitions can be evaluated, for this reason only molecular states that lead to such transitions are considered. Two Co states, $Co(3d^8 4s\ b^4F)$ and $Co(3d^8 4s\ b^4P)$, provide molecular states of both multiplicities and are included in both tables. Finally, the rate coefficients for 4862 partial inelastic processes in cobalt-hydrogen atomic collisions (in the neutral CoH system) and for 8190 partial inelastic processes in cobalt-hydrogen ionic collisions (in the ionized $CoH^+$ system), 13,052 partial processes in total, are calculated in the present work. One should note that not all processes are equally important. Previous NLTE studies have shown that inelastic H-collision processes with large values of the rate coefficients, mainly exceeding $10^{-8}$ cm$^3$/s, are most important, the processes with moderate rates, roughly between $10^{-12}$ and $10^{-8}$ cm$^3$/s, also rather important, while the processes with low rates, lower than $10^{-12}$ cm$^3$/s, are not important, see, e.g., [2,38–40] and references therein. Therefore, one needs to estimate rates for nearly all processes and to single out processes, which are important. In the present research this is done by means of the simplified model.

The present study of non-adiabatic nuclear dynamics is performed separately within the triplet and quintet molecular symmetries. Figure 1 presents the diabatic potential energies of the CoH quasimolecule. There are two kinds of diabatic potentials corresponding to ionic and to covalent molecular states. Since the simplified model is based on the asymptotic nature, the asymptotic diabatic potentials are determined by the dominant terms. Coulomb attractive potentials are used for ionic states. The diabatic potentials for covalent states are van der Waals potentials for neutral molecules and polarization potentials for charged molecules [31]. However the long-range part of these potentials differ little from the flat potentials [41]. For these reasons, the simplified model is using the flat potentials for covalent states [28,29]. Molecular states with different multiplicities are shown by

different colors and non-adiabatic transitions between states of the same molecular symmetry are considered since they are coupled by the radial matrix elements that provide the dominant mechanism for non-adiabatic transitions.

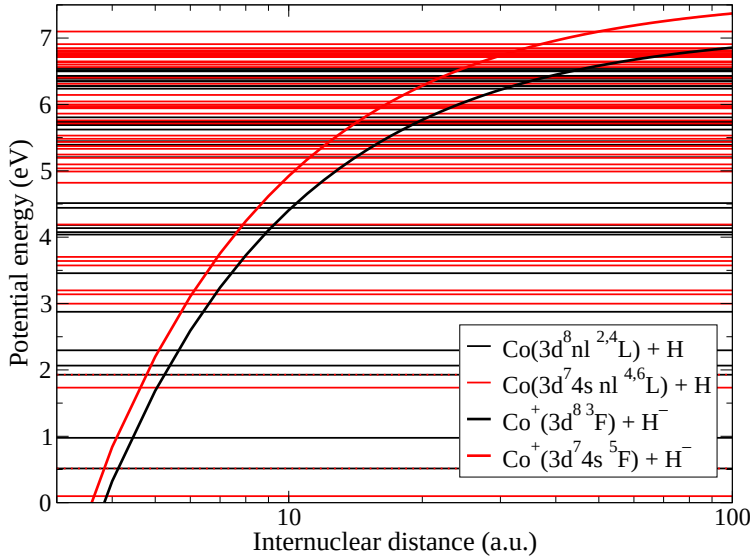


**Figure 1.** Diabatic potential energies for CoH. Molecular states with triplet multiplicity are shown by black lines, while states with quintet multiplicity by red lines.

Figure 2 shows the neutralization rate coefficients in collisions of $Co^+$ and $H^-$ as a function of the excitation energy. Both ground and first excited ionic states have several molecular symmetries, so the neutralization rate coefficients into covalent states of CoH that do not have all of the molecular symmetries identical to the corresponding ionic are smaller than the reduced rate coefficient from [28]. Please note that electron binding energies are measured from the ionic limit and are different for the cases of triplet and quintet states of CoH, this leads to two different lines for the reduced rate coefficients in Figure 2.

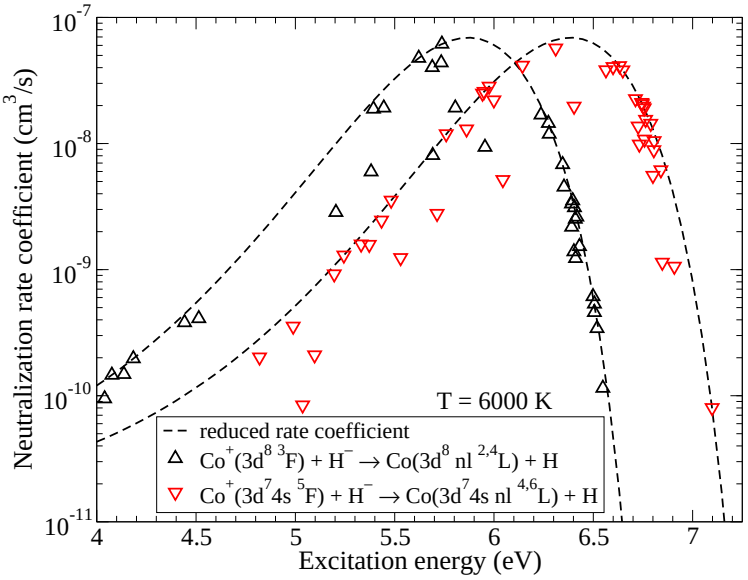


**Figure 2.** The rate coefficients for mutual neutralization in $Co^+ + H^-$ collisions as a function of the excitation energy. Dashed lines represent the reduced rate coefficients given by the simplified model.

Within triplet multiplicity, the highest rate coefficient at 6000 K corresponds to the mutual neutralization into the $Co(3d^8 5s\ e^2F) + H$ state ($j = 21$ in Table A1) with the value of $6.16 \times 10^{-8}$ cm$^3$/s. Within quintet multiplicity, the rate coefficient for the mutual neutralization into $Co(3d^7 4s4p\ y^4H^\circ) + H$ ($j = 32$ in Table A2) has the largest value of $5.7 \times 10^{-8}$ cm$^3$/s at 6000 K. It is seen from Figure 2 that the reduced rate coefficients reach their maximal values for the processes with the binding energies from the optimal window, around $-2$ eV, see [28], and decrease outside of the optimal window in both directions.

Rate coefficients for excitation and de-excitation processes have maximal values approximately by an order of magnitude smaller than the maximum values for the neutralization processes. The highest rate coefficients among them correspond to the de-excitation processes $Co(3d^8 4p\ y^2S^\circ) + H \rightarrow Co(3d^8 5s\ e^2F; 3d^8 4p\ v^4D^\circ) + H$ within triplet multiplicity ($i = 24 \rightarrow f = 21, 22$ in Table A1) with values around $8.1 \times 10^{-9}$ cm$^3$/s at 6000 K and $Co(3d^7 4s4p\ w^4P^\circ) + H \rightarrow Co(3d^7 4s4p\ y^4H^\circ) + H$ within quintet multiplicity ($i = 33 \rightarrow f = 32$ in Table A2) with the value $5.3 \times 10^{-9}$ cm$^3$/s at 6000 K. Electronic binding energies for the states involved in these processes are also close to $-2$ eV, this value corresponds to the maximum of the reduced rate coefficient for neutralization and de-excitation. The typical dependence of the (de)-excitation rate coefficients on the excitation energies is shown in Figure 3 for the initial channel $Co(3^8 5s\ e^2F) + H$ and the temperature $T = 6000$ K. As in the case of mutual neutralization, the scatter of the rate coefficients is due to the fact that not all molecular states lead to the same molecular symmetries in the initial and the final channels.

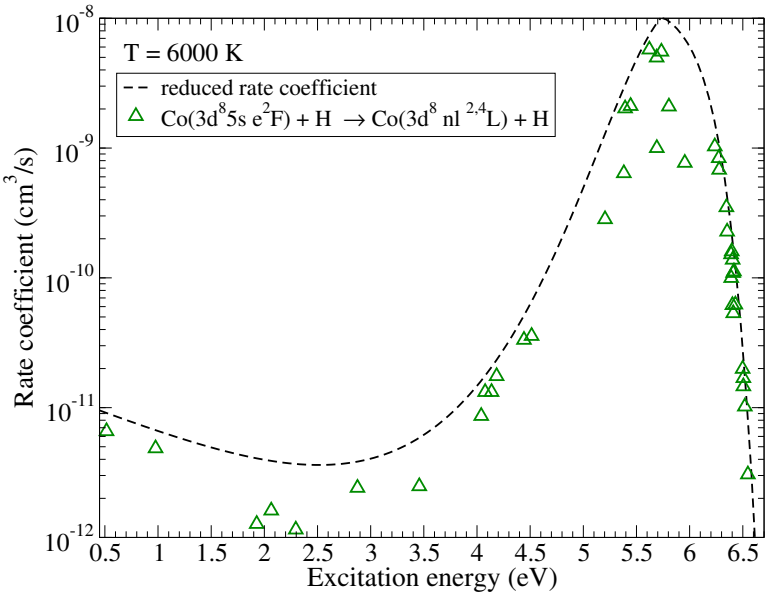


**Figure 3.** The rate coefficients for (de)-excitation in Co + H collisions as a function of the excitation energy at $T = 6000$ K. The initial channel is $Co(3d^8 5s\ e^2F) + H$. The dashed line represents the reduced rate coefficient given by the simplified model.

For the case of $CoH^+$, calculations are performed for 90 states of $Co^+ + H$ and the ground ionic state $Co^{2+}(3d^7\ ^4F) + H^-$. As the ionic state has $^4\Sigma^-$, $^4\Pi$, $^4\Delta$ and $^4\Phi$ molecular symmetries, only molecular states that have these symmetries are considered. The states are collected in Table A3. Rate coefficients are calculated within the simplified quantum model [29] that gives the general dependence of the rate coefficients in ionic collisions with hydrogen. As in case of the collisions of neutral atoms with hydrogen, only processes involving one-electron transitions are treated with this model.

Rate coefficients with the largest values correspond to the neutralization processes, they are shown in Figure 4 as a function of the excitation energy while the corresponding values of the electronic binding energy are plotted along the upper horizontal axis. The rate coefficient with

the largest value corresponds to the $Co^{2+}(3d^7\ ^4F) + H^- \rightarrow Co^+(3d^7 4d\ g^5F) + H$ process and is equal to $7.09 \times 10^{-8}$ cm$^3$/s at $T = 6000$ K. The final state of this process ($f = 58$) has all of the molecular symmetries identical to the ionic state and its electronic binding energy is close to $-4$ eV which corresponds to the maximum of the reduced rate coefficient for neutralization in collisions of double-charged positive ions with hydrogen negative ions.

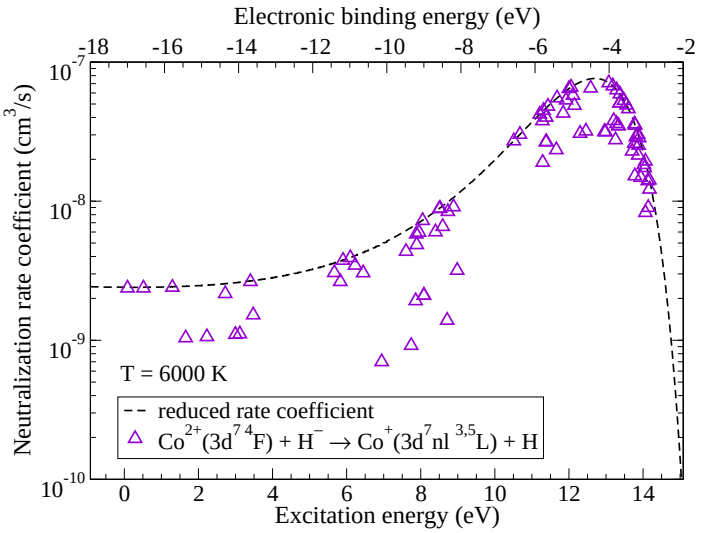


**Figure 4.** The rate coefficients for neutralization in $Co^{2+} + H^-$ collisions as a function of the excitation energy. Dashed line represents the reduced rate coefficient given by the simplified model.

Among the excitation and de-excitation, the highest rate coefficients correspond to the $Co^+(3d^7 4d\ h^3P) + H \rightarrow Co^+(3d^7 5s\ g^3P; 3d^7 4d\ g^5P; 3d^7 4d\ g^5F) + H$ processes (61 $\rightarrow$ 56, 57, 58 in Table A3) with values around $7 \times 10^{-9}$ cm$^3$/s at $T = 6000$ K. Electronic binding energies of these states are also close to $-4$ eV, maximum of the reduced rate coefficient for the collisions in $AH^+$ systems, see [29]. The typical dependence of the (de)-excitation rate coefficients on the excitation energies is shown in Figure 5 for the initial channel $Co(3d^7 4d\ g^5F) + H$ and at the temperature $T = 6000$ K.

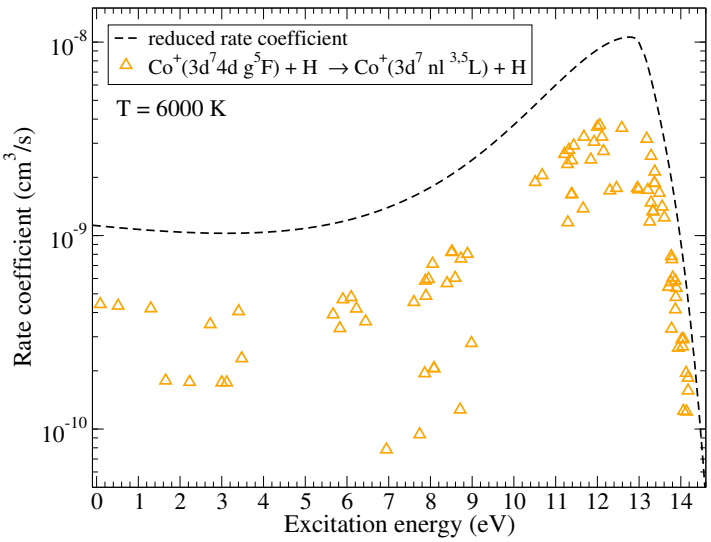


**Figure 5.** The rate coefficients for (de)-excitation processes in $Co^+ + H$ collisions as a function of the excitation energy at $T = 6000$ K. The initial channel is $Co^+(3d^7 4d\ g^5F) + H$. The dashed line represents the reduced rate coefficient given by the simplified model.

Thus, the rate coefficients calculated in the present work for the neutralization, ion-pair formation, excitation, and de-excitation processes in collisions Co + H, $Co^+ + H^-$, $Co^+$ + H, $Co^{2+} + H^-$ allow us to perform more accurate spectral line modeling for both Co I and Co II than ones based on the Drawin formula, which is known to be unreliable.

It is worth mentioning the electron-detachment process $Co^+ + H^- \rightarrow Co^+ + H + e$ which might be relevant to collisions treated, and which is energetically possible for collision energies above 0.75 eV. The low-energy electron detachment process typically should be treated within the local complex potential approximation of the projection-operator formalism, see, e.g., [42]. This requires treatment of two potentials: (i) an initial (ionic) discrete-state potential, and (ii) a final state potential with zero kinetic energy of an emitted electron, i.e., the $Co^+$ + H potential, which asymptotically is 0.75 eV above the ionic $Co^+ + H^-$ asymptote. If a discrete-state potential is embedded into the electronic continuum, then the discrete state becomes quasi-stationary, the discrete-state potential becomes complex, and the detachment process takes place. A simple diagram of these two potentials shows the following: the ionic Coulomb potential is strongly attractive, while the higher-lying $Co^+$ + H potential is a polarization potential, and hence, is weakly attractive. Therefore, the discrete-state potential cannot embedded into the electronic continuum at large and intermediate distances, it could happen at short-range only, leading to low-valued quasi-stationary width and to a low-valued cross section, much smaller than the neutralization cross section. For the reason of low cross sections (if any at all), this electron-detachment channel is not included into the list of final channels for $Co^+ + H^-$ and Co* + H collisions treated in the present study.

## 3. Spectral Line Modelling

We employ the NLTE model atom of Co developed in [21]. In brief, the model consists of 3 ionisation stages and 412 energy levels. 8,566 radiative transitions connect the energy levels in Co I and in Co II. The photo-ionisation for all levels were computed using the hydrogenic approximation. In [21], for the absence of detailed quantum-mechanical data, we employed the Drawin's formula [15,16] to compute the rates of bound-bound and bound-free transitions caused by inelastic collisions with H atoms.

The model atmospheres are taken from the MAFAGS-OS grid [43,44]. These are plane-parallel line-blanketed model atmospheres with convection approximated using the mixing length theory. We use the DETAIL statistical equilibrium code [45] and the SIU line formation code [46] to compute the NLTE number densities and emergent fluxes for selected Co I lines, which represent a useful abundance diagnostic in late-type stars.

The results of our calculations are shown in Figure 6 and presented in Table 1. For the turn-off models, these can be directly compared to Bergemann et al. [21] (their Table 4), as the only difference between our earlier calculations and this work is the implementation of new QM collision data with H atoms.

Clearly, the new collision rates have a very strong effect on the line formation and NLTE abundance corrections. For the solar-metallicity model at 6000 K and log(g)= 4 dex, our new NLTE abundance corrections are 3 times smaller compared to the older values. Also for the very metal-poor model of the TO star at [Fe/H] $= -2$, the effect is very large. The rate of thermalisation with the new H collision rates is much higher, leading to a significantly lower NLTE abundance corrections for the key Co I lines.

**Table 1.** NLTE abundance corrections for the four lines of neutral cobalt computed using the old model atom from Bergemann et al. 2010 and the new model atom from this paper. The parameters of stellar model atmospheres are given in the columns 1–3.

| $T_{eff}$ | log(g) | [Fe/H] | $V_{mic}$ | NLTE Corrections | | | |
|---|---|---|---|---|---|---|---|
| | | | | 4020 | 4110 | 4121 | 5369 |
| 4500 | 2.00 | 0.00 | 2.00 | 0.02 | 0.06 | 0.01 | 0.04 |
| 4500 | 2.00 | −2.00 | 2.00 | 0.24 | 0.43 | 0.27 | 0.20 |
| 6000 | 4.00 | 0.00 | 1.00 | 0.06 | 0.09 | 0.06 | 0.09 |
| 6000 | 4.00 | −2.00 | 1.00 | 0.40 | 0.27 | 0.28 | 0.24 |

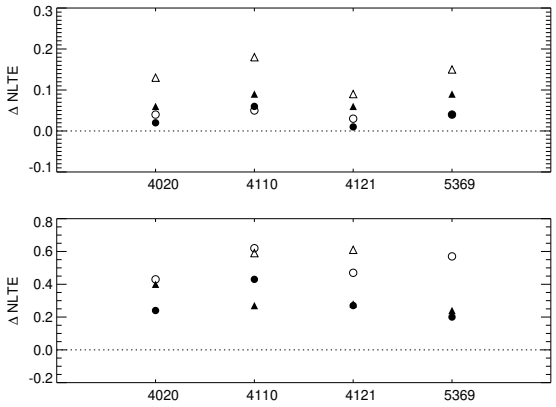


**Figure 6.** NLTE abundance corrections for four lines of Co I computed using the old model atom (open symbols) and the new model atom (filled symbols). The top panel presents the data for the metal-rich model atmospheres, [Fe/H] = 0, whereas the bottom panel illustrates the corrections for the very metal-poor models, [Fe/H] = −2. Triangles and circles correspond to a typical dwarf (Teff = 6000 K, log(g) = 4.0) and red giant (Teff = 4500 K, log(g) = 2.0) stellar model atmospheres, respectively.

## 4. Conclusions

Calculations of the rate coefficients for inelastic processes in low-energy Co + H, $Co^+ + H^-$, $Co^+ + H$, and $Co^{2+} + H^-$ collisions are performed by means of the quantum simplified model [28,29] can be found in Supplementary Materials. 44 triplet and 55 quintet states of CoH, as well as 91 states of $CoH^+$ are included into consideration. The calculations are performed separately for all molecular symmetries that are formed by the ionic states $Co^+(^3F) + H^-$, $Co^+(^5F) + H^-$ and $Co^{2+} + H^-$, as the long-range ionic-covalent interactions provide the dominant mechanism for non-adiabatic transitions.

The rate coefficients are calculated for the 4862 partial processes (mutual neutralization, ion-pair formation, excitation and de-excitation) in the neutral CoH system, and for the 8190 partial processes in the ionized $CoH^+$ system, 13,052 processes in total.

The largest rate coefficients correspond to neutralization processes in both the neutral and the ionized collisional systems. In $Co^+ + H^-$ collisions, at $T = 6000$ K, the largest values are $6.16 \times 10^{-8}$ cm$^3$/s for $Co^+(3d^8\ ^3F) + H^- \rightarrow Co(3d^8 5s\ e^2F) + H$ (transitions in the triplet system) and $5.7 \times 10^{-8}$ cm$^3$/s for $Co^+(3d^7 4s\ ^5F) + H^- \rightarrow Co(3d^7 4s4p\ y^4H^\circ) + H$ (transitions in the quintet system). In $Co^{2+} + H^-$ collisions, at $T = 6000$ K, the largest values are $7.09 \times 10^{-8}$ cm$^3$/s for the $Co^{2+}(3d^7\ ^4F) + H^- \rightarrow Co^+(3d^7 4d\ g^5F) + H$ process. Among the excitation and de-excitation processes, the largest rate coefficients at $T = 6000$ K have the values around $8.1 \times 10^{-9}$ cm$^3$/s for the neutral system corresponding to $Co(3d^8 4p\ y^2S^\circ) + H \rightarrow Co(3d^8 5s\ e^2F; 3d^8 4p\ v^4D^\circ) + H$ processes and around $7 \times 10^{-9}$ cm$^3$/s for the ionic system corresponding to $Co^+(3d^7 4d\ h^3P) + H \rightarrow Co^+(3d^7 5s\ g^3P; 3d^7 4d\ g^5P; 3d^7 4d\ g^5F) + H$ processes. That is, the maximal rates for excitation and de-excitation processes are roughly by an order of magnitude smaller than the maximal rates for neutralization processes. All these inelastic processes have the binding energies which belong to the optimal windows, i.e., to the binding energy ranges which provide the largest rate coefficients,

as predicted by the simplified model [28,29]. The large-valued rate coefficients are determined with rather high accuracy, and they are expected to be important for NLTE stellar atmosphere modelling. Outside of the optimal windows in both directions, the rate coefficients decrease, as well as their accuracy. As shown earlier, see, e.g., [31], for inelastic processes with low-valued rate coefficients, other reaction mechanisms, in particular, related to short-range nonadiabatic regions, become more important (might be even dominant), so accounting for other reaction mechanisms might increase low-valued rates substantially.

It should be noted that cobalt is a relatively heavy atom, and spin-orbit interaction can be significant, especially for low-lying states. However, the account for fine structure of the colliding partners is a very complicated problem and beyond the scope of the present paper. For accounting of the fine structures in collisions alcali-like atoms and ions with hydrogen see Belyaev et al. [47].

We performed test NLTE calculations for selected stellar model atmospheres using the H-collisional data obtained in the present work. We compared the results of these calculations with our previous results [21]. To maintain consistency in the comparative analysis, the only difference between the earlier calculations and this work is the implementation of the new quantum H-collision data. We found that the influence of cobalt-hydrogen collisions has an important effect on the line formation of Co I lines and on NLTE abundance corrections (Figure 6). The sign of the NLTE abundance corrections does not change: they are strictly positive and increase with increasing $T_{\rm eff}$ and decreasing metallicity. Our model atom [21] predicted large NLTE corrections for metal-poor stars, up to $+0.6$ dex at $[{\rm Fe/H}] = -2$. With the new model, the NLTE abundance corrections appear to be a factor of two smaller compared to the previous estimates. Nonetheless, the NLTE effects at low metallicity, $[{\rm Fe/H}] = -2$, are significant and range from 0.25 dex for the Co I line at 5369 Å to 0.40 for the 4020 Å line. This result suggests that the NLTE effects in Co I lines are strong and must be included in accurate abundance analyses of cool stars.

**Supplementary Materials:** The following are available online at http://www.mdpi.com/2218-2004/8/3/34/s1.

**Author Contributions:** Data calculations, S.A.Y.; data analysis, S.A.Y. and A.K.B.; data curation, A.K.B. and S.A.Y.; astrophysical applications, M.B.; writing, S.A.Y., A.K.B., and M.B. All authors have read and agreed to the published version of the manuscript. Authorship is limited to those who have contributed substantially to the work reported.

**Acknowledgments:** S.A.Y. and A.K.B. gratefully acknowledge support from the Ministry of Education of the Russian Federation (project FSZN-2020-0026).

**Conflicts of Interest:** The authors declare no conflict of interest.

## Abbreviations

The following abbreviations are used in this manuscript:

| | |
|---|---|
| [H] LTE | Local Thermodynamic Equilibrium |
| NLTE | Non-Local Thermodynamic Equilibrium |
| SN | Supernova |
| dSph galaxy | dwarf spheroidal galaxy |

## Appendix A

The scattering channels and the corresponding molecular states treated in the present work are collected in Tables A1–A3 for the CoH and $CoH^+$ collisional systems.

**Table A1.** Scattering channels correlated with CoH molecular triplet states, the asymptotic excitation energies ($J$-averaged experimental values taken from NIST [48]) with respect to the ground state, and their molecular symmetries.

| j | Scattering Channels | Excitation Energy (eV) | Molecular Symmetries | | | |
|---|---|---|---|---|---|---|
| 1 | $Co(3d^8 4s\ b^4F) + H$ | 0.51548 | $^3\Sigma^-$ | $^3\Pi$ | $^3\Delta$ | $^3\Phi$ |
| 2 | $Co(3d^8 4s\ a^2F) + H$ | 0.97685 | $^3\Sigma^-$ | $^3\Pi$ | $^3\Delta$ | $^3\Phi$ |
| 3 | $Co(3d^8 4s\ b^4P) + H$ | 1.92787 | $^3\Sigma^-$ | $^3\Pi$ | | |
| 4 | $Co(3d^8 4s\ a^2D) + H$ | 2.06497 | | $^3\Pi$ | $^3\Delta$ | |
| 5 | $Co(3d^8 4s\ a^2P) + H$ | 2.29594 | $^3\Sigma^-$ | $^3\Pi$ | | |
| 6 | $Co(3d^8 4s\ b^2G) + H$ | 2.87577 | | $^3\Pi$ | $^3\Delta$ | $^3\Phi$ |
| 7 | $Co(3d^9\ c^2D) + H$ | 3.45747 | | $^3\Pi$ | $^3\Delta$ | |
| 8 | $Co(3d^8 4p\ y^4D^\circ) + H$ | 4.03969 | $^3\Sigma^-$ | $^3\Pi$ | $^3\Delta$ | |
| 9 | $Co(3d^8 4p\ y^4G^\circ) + H$ | 4.07631 | $^3\Sigma^-$ | $^3\Pi$ | $^3\Delta$ | $^3\Phi$ |
| 10 | $Co(3d^8 4p\ y^4F^\circ) + H$ | 4.13694 | | $^3\Pi$ | $^3\Delta$ | $^3\Phi$ |
| 11 | $Co(3d^8 4p\ y^2G^\circ) + H$ | 4.18423 | $^3\Sigma^-$ | $^3\Pi$ | $^3\Delta$ | $^3\Phi$ |
| 12 | $Co(3d^8 4p\ y^2F^\circ) + H$ | 4.44203 | | $^3\Pi$ | $^3\Delta$ | $^3\Phi$ |
| 13 | $Co(3d^8 4p\ y^2D^\circ) + H$ | 4.51371 | $^3\Sigma^-$ | $^3\Pi$ | $^3\Delta$ | |
| 14 | $Co(3d^8 4p\ z^4P^\circ) + H$ | 5.20406 | | $^3\Pi$ | | |
| 15 | $Co(3d^8 4p\ z^2P^\circ) + H$ | 5.38114 | | $^3\Pi$ | | |
| 16 | $Co(3d^8 4p\ x^2F^\circ) + H$ | 5.39327 | | $^3\Pi$ | $^3\Delta$ | $^3\Phi$ |
| 17 | $Co(3d^8 4p\ x^2D^\circ) + H$ | 5.44509 | $^3\Sigma^-$ | $^3\Pi$ | $^3\Delta$ | |
| 18 | $Co(3d^8 5s\ e^4F) + H$ | 5.62102 | $^3\Sigma^-$ | $^3\Pi$ | $^3\Delta$ | $^3\Phi$ |
| 19 | $Co(3d^8 4p\ w^2D^\circ) + H$ | 5.68931 | $^3\Sigma^-$ | $^3\Pi$ | $^3\Delta$ | |
| 20 | $Co(3d^8 4p\ y^4S^\circ) + H$ | 5.69145 | $^3\Sigma^-$ | | | |
| 21 | $Co(3d^8 5s\ e^2F) + H$ | 5.73759 | $^3\Sigma^-$ | $^3\Pi$ | $^3\Delta$ | $^3\Phi$ |
| 22 | $Co(3d^8 4p\ v^4D^\circ) + H$ | 5.73428 | $^3\Sigma^-$ | $^3\Pi$ | $^3\Delta$ | |
| 23 | $Co(3d^8 4p\ y^2P^\circ) + H$ | 5.80502 | | $^3\Pi$ | | |
| 24 | $Co(3d^8 4p\ y^2S^\circ) + H$ | 5.95449 | $^3\Sigma^-$ | | | |
| 25 | $Co(3d^8 4p\ y^2H^\circ) + H$ | 6.23651 | | $^3\Pi$ | $^3\Delta$ | $^3\Phi$ |
| 26 | $Co(3d^8 4p\ w^2G^\circ) + H$ | 6.27376 | $^3\Sigma^-$ | $^3\Pi$ | $^3\Delta$ | $^3\Phi$ |
| 27 | $Co(3d^8 4p\ u^2F^\circ) + H$ | 6.27806 | | $^3\Pi$ | $^3\Delta$ | $^3\Phi$ |
| 28 | $Co(3d^8 5p\ v^2G^\circ) + H$ | 6.34547 | $^3\Sigma^-$ | $^3\Pi$ | $^3\Delta$ | $^3\Phi$ |
| 29 | $Co(3d^8 5p\ s^4D^\circ) + H$ | 6.35225 | $^3\Sigma^-$ | $^3\Pi$ | $^3\Delta$ | |
| 30 | $Co(3d^8 5p\ u^4F^\circ) + H$ | 6.38987 | | $^3\Pi$ | $^3\Delta$ | $^3\Phi$ |
| 31 | $Co(3d^8 4d\ e^4D) + H$ | 6.39093 | | $^3\Pi$ | $^3\Delta$ | |
| 32 | $Co(3d^8 4d\ g^4F) + H$ | 6.39638 | $^3\Sigma^-$ | $^3\Pi$ | $^3\Delta$ | $^3\Phi$ |
| 33 | $Co(3d^8 4d\ e^4P) + H$ | 6.40229 | $^3\Sigma^-$ | $^3\Pi$ | | |
| 34 | $Co(3d^8 4d\ e^4H) + H$ | 6.40499 | $^3\Sigma^-$ | $^3\Pi$ | $^3\Delta$ | $^3\Phi$ |
| 35 | $Co(3d^8 4d\ e^4G) + H$ | 6.40948 | | $^3\Pi$ | $^3\Delta$ | $^3\Phi$ |
| 36 | $Co(3d^8 4d\ e^2P) + H$ | 6.41068 | $^3\Sigma^-$ | $^3\Pi$ | | |
| 37 | $Co(3d^8 5p\ u^4G^\circ) + H$ | 6.41689 | $^3\Sigma^-$ | $^3\Pi$ | $^3\Delta$ | $^3\Phi$ |
| 38 | $Co(3d^8 5p\ t^2D^\circ) + H$ | 6.43021 | $^3\Sigma^-$ | $^3\Pi$ | $^3\Delta$ | |
| 39 | $Co(3d^8 4d\ e^2H) + H$ | 6.49858 | $^3\Sigma^-$ | $^3\Pi$ | $^3\Delta$ | $^3\Phi$ |
| 40 | $Co(3d^8 4d\ e^2G) + H$ | 6.50516 | | $^3\Pi$ | $^3\Delta$ | $^3\Phi$ |
| 41 | $Co(3d^8 4d\ f^2F) + H$ | 6.50548 | $^3\Sigma^-$ | $^3\Pi$ | $^3\Delta$ | $^3\Phi$ |
| 42 | $Co(3d^8 5p\ s^2F^\circ) + H$ | 6.51886 | | $^3\Pi$ | $^3\Delta$ | $^3\Phi$ |
| 43 | $Co(3d^8 4d\ e^2D) + H$ | 6.54802 | | $^3\Pi$ | $^3\Delta$ | |
| 44 | $Co^+(3d^8\ ^3F) + H^-$ | 7.12701 | $^3\Sigma^-$ | $^3\Pi$ | $^3\Delta$ | $^3\Phi$ |

**Table A2.** Scattering channels correlated with CoH molecular quintet states, the asymptotic excitation energies ($J$-averaged experimental values taken from NIST [48]) with respect to the ground state, and their molecular symmetries.

| j | Scattering Channels | Excitation Energy (eV) | Molecular Symmetries | | | |
|---|---|---|---|---|---|---|
| 1 | $Co(3d^7 4s^2\ a^4F) + H$ | 0.09833 | $^5\Sigma^-$ | $^5\Pi$ | $^5\Delta$ | $^5\Phi$ |
| 2 | $Co(3d^8 4s\ b^4F) + H$ | 0.51548 | $^5\Sigma^-$ | $^5\Pi$ | $^5\Delta$ | $^5\Phi$ |
| 3 | $Co(3d^7 4s^2\ a^4P) + H$ | 1.73285 | $^5\Sigma^-$ | $^5\Pi$ | | |
| 4 | $Co(3d^8 4s\ b^4P) + H$ | 1.92787 | $^5\Sigma^-$ | $^5\Pi$ | | |
| 5 | $Co(3d^7 4s4p\ z^6F^\circ) + H$ | 2.99786 | | $^5\Pi$ | $^5\Delta$ | $^5\Phi$ |
| 6 | $Co(3d^7 4s4p\ z^6D^\circ) + H$ | 3.13938 | $^5\Sigma^-$ | $^5\Pi$ | $^5\Delta$ | |
| 7 | $Co(3d^7 4s4p\ z^6G^\circ) + H$ | 3.19854 | $^5\Sigma^-$ | $^5\Pi$ | $^5\Delta$ | $^5\Phi$ |
| 8 | $Co(3d^7 4s4p\ z^4F^\circ) + H$ | 3.57441 | | $^5\Pi$ | $^5\Delta$ | $^5\Phi$ |
| 9 | $Co(3d^7 4s4p\ z^4G^\circ) + H$ | 3.64148 | $^5\Sigma^-$ | $^5\Pi$ | $^5\Delta$ | $^5\Phi$ |
| 10 | $Co(3d^7 4s4p\ z^4D^\circ) + H$ | 3.70284 | $^5\Sigma^-$ | $^5\Pi$ | $^5\Delta$ | |
| 11 | $Co(3d^7 4s4p\ z^6S^\circ) + H$ | 4.19102 | $^5\Sigma^-$ | | | |
| 12 | $Co(3d^7 4s4p\ y^6D^\circ) + H$ | 4.81956 | $^5\Sigma^-$ | $^5\Pi$ | $^5\Delta$ | |
| 13 | $Co(3d^7 4s4p\ x^4D^\circ) + H$ | 4.98902 | $^5\Sigma^-$ | $^5\Pi$ | $^5\Delta$ | |
| 14 | $Co(3d^7 4s4p\ z^4S^\circ) + H$ | 5.03644 | $^5\Sigma^-$ | | | |
| 15 | $Co(3d^7 4s4p\ z^6P^\circ) + H$ | 5.09679 | | $^5\Pi$ | | |
| 16 | $Co(3d^7 4s4p\ x^4F^\circ) + H$ | 5.19581 | | $^5\Pi$ | $^5\Delta$ | $^5\Phi$ |
| 17 | $Co(3d^7 4s4p\ x^4G^\circ) + H$ | 5.24427 | $^5\Sigma^-$ | $^5\Pi$ | $^5\Delta$ | $^5\Phi$ |
| 18 | $Co(3d^7 4s4p\ z^4H^\circ) + H$ | 5.33119 | | $^5\Pi$ | $^5\Delta$ | $^5\Phi$ |
| 19 | $Co(3d^7 4s4p\ w^4D^\circ) + H$ | 5.37206 | $^5\Sigma^-$ | $^5\Pi$ | $^5\Delta$ | |
| 20 | $Co(3d^7 4s4p\ w^4F^\circ) + H$ | 5.43392 | | $^5\Pi$ | $^5\Delta$ | $^5\Phi$ |
| 21 | $Co(3d^7 4s4p\ w^4G^\circ) + H$ | 5.48224 | $^5\Sigma^-$ | $^5\Pi$ | $^5\Delta$ | $^5\Phi$ |
| 22 | $Co(3d^7 4s4p\ y^4P^\circ) + H$ | 5.52998 | | $^5\Pi$ | | |
| 23 | $Co(3d^7 4s4p\ x^4P^\circ) + H$ | 5.71331 | | $^5\Pi$ | | |
| 24 | $Co(3d^7 4s5s\ e^6F) + H$ | 5.75952 | $^5\Sigma^-$ | $^5\Pi$ | $^5\Delta$ | $^5\Phi$ |
| 25 | $Co(3d^7 4s4p\ u^4D^\circ) + H$ | 5.86199 | $^5\Sigma^-$ | $^5\Pi$ | $^5\Delta$ | |
| 26 | $Co(3d^7 4s4p\ v^4G^\circ) + H$ | 5.94217 | $^5\Sigma^-$ | $^5\Pi$ | $^5\Delta$ | $^5\Phi$ |
| 27 | $Co(3d^7 4s5s\ f^4F) + H$ | 5.97552 | $^5\Sigma^-$ | $^5\Pi$ | $^5\Delta$ | $^5\Phi$ |
| 28 | $Co(3d^7 4s4p\ t^4D^\circ) + H$ | 5.99915 | $^5\Sigma^-$ | $^5\Pi$ | $^5\Delta$ | |
| 29 | $Co(3d^7 4s4p\ z^4I^\circ) + H$ | 5.95034 | $^5\Sigma^-$ | $^5\Pi$ | $^5\Delta$ | $^5\Phi$ |
| 30 | $Co(3d^7 4s4p\ x^4S^\circ) + H$ | 6.04469 | $^5\Sigma^-$ | | | |
| 31 | $Co(3d^7 4s4p\ v^4F^\circ) + H$ | 6.14320 | | $^5\Pi$ | $^5\Delta$ | $^5\Phi$ |
| 32 | $Co(3d^7 4s4p\ y^4H^\circ) + H$ | 6.31054 | | $^5\Pi$ | $^5\Delta$ | $^5\Phi$ |
| 33 | $Co(3d^7 4s4p\ w^4P^\circ) + H$ | 6.40304 | | $^5\Pi$ | | |
| 34 | $Co(3d^7 4s5p\ x^6D^\circ) + H$ | 6.56348 | $^5\Sigma^-$ | $^5\Pi$ | $^5\Delta$ | |
| 35 | $Co(3d^7 4s5p\ y^6F^\circ) + H$ | 6.59929 | | $^5\Pi$ | $^5\Delta$ | $^5\Phi$ |
| 36 | $Co(3d^7 4s5p\ y^6G^\circ) + H$ | 6.63201 | $^5\Sigma^-$ | $^5\Pi$ | $^5\Delta$ | $^5\Phi$ |
| 37 | $Co(3d^7 4s5s\ h^4F) + H$ | 6.64847 | $^5\Sigma^-$ | $^5\Pi$ | $^5\Delta$ | $^5\Phi$ |
| 38 | $Co(3d^7 4s4d\ f^4G) + H$ | 6.71229 | | $^5\Pi$ | $^5\Delta$ | $^5\Phi$ |
| 39 | $Co(3d^7 4s4d\ f^4D) + H$ | 6.72580 | | $^5\Pi$ | $^5\Delta$ | |
| 40 | $Co(3d^7 4s4d\ e^6P) + H$ | 6.73166 | $^5\Sigma^-$ | $^5\Pi$ | | |
| 41 | $Co(3d^7 4s4d\ f^4H) + H$ | 6.74361 | $^5\Sigma^-$ | $^5\Pi$ | $^5\Delta$ | $^5\Phi$ |
| 42 | $Co(3d^7 4s5p\ t^4G^\circ) + H$ | 6.74639 | $^5\Sigma^-$ | $^5\Pi$ | $^5\Delta$ | $^5\Phi$ |
| 43 | $Co(3d^7 4s4d\ i^4F) + H$ | 6.75237 | $^5\Sigma^-$ | $^5\Pi$ | $^5\Delta$ | $^5\Phi$ |
| 44 | $Co(3d^7 4s4d\ f^6F) + H$ | 6.75635 | $^5\Sigma^-$ | $^5\Pi$ | $^5\Delta$ | $^5\Phi$ |
| 45 | $Co(3d^7 4s4d\ e^6D) + H$ | 6.75759 | | $^5\Pi$ | $^5\Delta$ | |
| 46 | $Co(3d^7 4s4d\ e^6G) + H$ | 6.76313 | | $^5\Pi$ | $^5\Delta$ | $^5\Phi$ |
| 47 | $Co(3d^7 4s4d\ e^6H) + H$ | 6.78897 | $^5\Sigma^-$ | $^5\Pi$ | $^5\Delta$ | $^5\Phi$ |
| 48 | $Co(3d^7 4s4d\ f^4P) + H$ | 6.80010 | $^5\Sigma^-$ | $^5\Pi$ | | |
| 49 | $Co(3d^7 4s5p\ r^4D^\circ) + H$ | 6.80463 | $^5\Sigma^-$ | $^5\Pi$ | $^5\Delta$ | |
| 50 | $Co(3d^7 4s5p\ t^4F^\circ) + H$ | 6.80604 | | $^5\Pi$ | $^5\Delta$ | $^5\Phi$ |
| 51 | $Co(3d^7 4s4p\ q^4D^\circ) + H$ | 6.84015 | $^5\Sigma^-$ | $^5\Pi$ | $^5\Delta$ | |
| 52 | $Co(3d^7 4s4p\ w^4S^\circ) + H$ | 6.84726 | $^5\Sigma^-$ | | | |
| 53 | $Co(3d^7 4s4p\ v^4P^\circ) + H$ | 6.90793 | | $^5\Pi$ | | |
| 54 | $Co(3d^7 4s6s\ g^6F) + H$ | 7.09831 | $^5\Sigma^-$ | $^5\Pi$ | $^5\Delta$ | $^5\Phi$ |
| 55 | $Co^+(3d^7 4s\ ^5F) + H^-$ | 7.64209 | $^5\Sigma^-$ | $^5\Pi$ | $^5\Delta$ | $^5\Phi$ |

**Table A3.** Scattering channels correlated with $CoH^+$ molecular states, the asymptotic excitation energies ($J$-averaged experimental values taken from NIST [48]) with respect to the ground state, and their molecular symmetries.

| j | Scattering Channels | Excitation Energy (eV) | Molecular Symmetries | | | |
|---|---|---|---|---|---|---|
| 1 | $Co^+(3d^8\ a^3F) + H$ | 0.086424 | $^4\Sigma^-$ | $^4\Pi$ | $^4\Delta$ | $^4\Phi$ |
| 2 | $Co^+(3d^7 4s\ a^5F) + H$ | 0.515088 | $^4\Sigma^-$ | $^4\Pi$ | $^4\Delta$ | $^4\Phi$ |
| 3 | $Co^+(3d^7 4s\ b^3F) + H$ | 1.298194 | $^4\Sigma^-$ | $^4\Pi$ | $^4\Delta$ | $^4\Phi$ |
| 4 | $Co^+(3d^8\ a^3P) + H$ | 1.654634 | $^4\Sigma^-$ | $^4\Pi$ | | |
| 5 | $Co^+(3d^7 4s\ a^5P) + H$ | 2.228192 | $^4\Sigma^-$ | $^4\Pi$ | | |
| 6 | $Co^+(3d^7 4s\ a^3G) + H$ | 2.722395 | | $^4\Pi$ | $^4\Delta$ | $^4\Phi$ |
| 7 | $Co^+(3d^7 4s\ b^3P) + H$ | 2.997467 | $^4\Sigma^-$ | $^4\Pi$ | | |
| 8 | $Co^+(3d^7 4s\ c^3P) + H$ | 3.116769 | $^4\Sigma^-$ | $^4\Pi$ | | |
| 9 | $Co^+(3d^7 4s\ a^3H) + H$ | 3.402627 | $^4\Sigma^-$ | $^4\Pi$ | $^4\Delta$ | $^4\Phi$ |
| 10 | $Co^+(3d^7 4s\ a^3D) + H$ | 3.477810 | | $^4\Pi$ | $^4\Delta$ | |
| 11 | $Co^+(3d^7 4p\ z^5F^\circ) + H$ | 5.667889 | | $^4\Pi$ | $^4\Delta$ | $^4\Phi$ |
| 12 | $Co^+(3d^7 4p\ z^5D^\circ) + H$ | 5.829194 | $^4\Sigma^-$ | $^4\Pi$ | $^4\Delta$ | |
| 13 | $Co^+(3d^7 4p\ z^5G^\circ) + H$ | 5.901901 | $^4\Sigma^-$ | $^4\Pi$ | $^4\Delta$ | $^4\Phi$ |
| 14 | $Co^+(3d^7 4p\ z^3G^\circ) + H$ | 6.100510 | $^4\Sigma^-$ | $^4\Pi$ | $^4\Delta$ | $^4\Phi$ |
| 15 | $Co^+(3d^7 4p\ z^3F^\circ) + H$ | 6.225915 | | $^4\Pi$ | $^4\Delta$ | $^4\Phi$ |
| 16 | $Co^+(3d^7 4p\ z^3D^\circ) + H$ | 6.445432 | $^4\Sigma^-$ | $^4\Pi$ | $^4\Delta$ | |
| 17 | $Co^+(3d^7 4p\ z^5S^\circ) + H$ | 6.944416 | $^4\Sigma^-$ | | | |
| 18 | $Co^+(3d^7 4p\ y^5D^\circ) + H$ | 7.602664 | $^4\Sigma^-$ | $^4\Pi$ | $^4\Delta$ | |
| 19 | $Co^+(3d^7 4p\ z^3S^\circ) + H$ | 7.741586 | $^4\Sigma^-$ | | | |
| 20 | $Co^+(3d^7 4p\ z^3H^\circ) + H$ | 7.879665 | | $^4\Pi$ | $^4\Delta$ | $^4\Phi$ |
| 21 | $Co^+(3d^7 4p\ z^5P^\circ) + H$ | 7.862606 | | $^4\Pi$ | | |
| 22 | $Co^+(3d^7 4p\ y^3F^\circ) + H$ | 7.953864 | | $^4\Pi$ | $^4\Delta$ | $^4\Phi$ |
| 23 | $Co^+(3d^7 4p\ y^3D^\circ) + H$ | 7.891881 | $^4\Sigma^-$ | $^4\Pi$ | $^4\Delta$ | |
| 24 | $Co^+(3d^7 4p\ y^3G^\circ) + H$ | 8.050841 | $^4\Sigma^-$ | $^4\Pi$ | $^4\Delta$ | $^4\Phi$ |
| 25 | $Co^+(3d^7 4p\ z^3P^\circ) + H$ | 8.082848 | | $^4\Pi$ | | |
| 26 | $Co^+(3d^7 4p\ y^3P^\circ) + H$ | 8.087312 | | $^4\Pi$ | | |
| 27 | $Co^+(3d^7 4p\ x^3D^\circ) + H$ | 8.396528 | $^4\Sigma^-$ | $^4\Pi$ | $^4\Delta$ | |
| 28 | $Co^+(3d^7 4p\ z^3I^\circ) + H$ | 8.502082 | $^4\Sigma^-$ | $^4\Pi$ | $^4\Delta$ | $^4\Phi$ |
| 29 | $Co^+(3d^7 4p\ x^3G^\circ) + H$ | 8.519635 | $^4\Sigma^-$ | $^4\Pi$ | $^4\Delta$ | $^4\Phi$ |
| 30 | $Co^+(3d^7 4p\ w^3D^\circ) + H$ | 8.592569 | $^4\Sigma^-$ | $^4\Pi$ | $^4\Delta$ | |
| 31 | $Co^+(3d^7 4p\ y^3S^\circ) + H$ | 8.711866 | $^4\Sigma^-$ | | | |
| 32 | $Co^+(3d^7 4p\ x^3F^\circ) + H$ | 8.730561 | | $^4\Pi$ | $^4\Delta$ | $^4\Phi$ |
| 33 | $Co^+(3d^7 4p\ y^3H^\circ) + H$ | 8.885763 | | $^4\Pi$ | $^4\Delta$ | $^4\Phi$ |
| 34 | $Co^+(3d^7 4p\ x^3P^\circ) + H$ | 8.983867 | | $^4\Pi$ | | |
| 35 | $Co^+(3d^7 5s\ e^5F) + H$ | 10.51110 | $^4\Sigma^-$ | $^4\Pi$ | $^4\Delta$ | $^4\Phi$ |
| 36 | $Co^+(3d^7 5s\ e^3F) + H$ | 10.67719 | $^4\Sigma^-$ | $^4\Pi$ | $^4\Delta$ | $^4\Phi$ |
| 37 | $Co^+(3d^7 4d\ f^5F) + H$ | 11.21252 | $^4\Sigma^-$ | $^4\Pi$ | $^4\Delta$ | $^4\Phi$ |
| 38 | $Co^+(3d^7 4d\ e^5G) + H$ | 11.28284 | | $^4\Pi$ | $^4\Delta$ | $^4\Phi$ |
| 39 | $Co^+(3d^7 4d\ e^5P) + H$ | 11.29226 | $^4\Sigma^-$ | $^4\Pi$ | | |
| 40 | $Co^+(3d^7 4d\ e^5H) + H$ | 11.31398 | $^4\Sigma^-$ | $^4\Pi$ | $^4\Delta$ | $^4\Phi$ |
| 41 | $Co^+(3d^7 4d\ e^5D) + H$ | 11.37796 | | $^4\Pi$ | $^4\Delta$ | |
| 42 | $Co^+(3d^7 4d\ e^3G) + H$ | 11.38589 | | $^4\Pi$ | $^4\Delta$ | $^4\Phi$ |
| 43 | $Co^+(3d^7 4d\ e^3D) + H$ | 11.39005 | | $^4\Pi$ | $^4\Delta$ | |
| 44 | $Co^+(3d^7 4d\ e^3H) + H$ | 11.43308 | $^4\Sigma^-$ | $^4\Pi$ | $^4\Delta$ | $^4\Phi$ |
| 45 | $Co^+(3d^7 4d\ e^3P) + H$ | 11.65906 | $^4\Sigma^-$ | $^4\Pi$ | | |
| 46 | $Co^+(3d^7 4d\ f^3F) + H$ | 11.67783 | $^4\Sigma^-$ | $^4\Pi$ | $^4\Delta$ | $^4\Phi$ |
| 47 | $Co^+(3d^7 5p\ x^5D^\circ) + H$ | 11.84426 | $^4\Sigma^-$ | $^4\Pi$ | $^4\Delta$ | |
| 48 | $Co^+(3d^7 5p\ y^5F^\circ) + H$ | 11.92089 | | $^4\Pi$ | $^4\Delta$ | $^4\Phi$ |
| 49 | $Co^+(3d^7 5p\ y^5G^\circ) + H$ | 12.00107 | $^4\Sigma^-$ | $^4\Pi$ | $^4\Delta$ | $^4\Phi$ |
| 50 | $Co^+(3d^7 5p\ w^3G^\circ) + H$ | 12.05815 | $^4\Sigma^-$ | $^4\Pi$ | $^4\Delta$ | $^4\Phi$ |

| j | Scattering Channels | Excitation Energy (eV) | Molecular Symmetries | | | |
|---|---|---|---|---|---|---|
| 51 | $Co^+(3d^7 5p\ w^3F^\circ) + H$ | 12.10782 | | $^4\Pi$ | $^4\Delta$ | $^4\Phi$ |
| 52 | $Co^+(3d^7 5p\ v^3D^\circ) + H$ | 12.14754 | $^4\Sigma^-$ | $^4\Pi$ | $^4\Delta$ | |
| 53 | $Co^+(3d^7 5s\ f^5P) + H$ | 12.29916 | $^4\Sigma^-$ | $^4\Pi$ | | |
| 54 | $Co^+(3d^7 5s\ f^3P) + H$ | 12.45811 | $^4\Sigma^-$ | $^4\Pi$ | | |
| 55 | $Co^+(3d^7 5s\ f^3G) + H$ | 12.58565 | | $^4\Pi$ | $^4\Delta$ | $^4\Phi$ |
| 56 | $Co^+(3d^7 5s\ g^3P) + H$ | 12.95788 | $^4\Sigma^-$ | $^4\Pi$ | | |
| 57 | $Co^+(3d^7 4d\ g^5P) + H$ | 12.98524 | $^4\Sigma^-$ | $^4\Pi$ | | |
| 58 | $Co^+(3d^7 4d\ g^5F) + H$ | 13.07439 | $^4\Sigma^-$ | $^4\Pi$ | $^4\Delta$ | $^4\Phi$ |
| 59 | $Co^+(3d^7 4d\ g^3F) + H$ | 13.18202 | $^4\Sigma^-$ | $^4\Pi$ | $^4\Delta$ | $^4\Phi$ |
| 60 | $Co^+(3d^7 4d\ f^5D) + H$ | 13.20781 | | $^4\Pi$ | $^4\Delta$ | |
| 61 | $Co^+(3d^7 4d\ h^3P) + H$ | 13.25611 | $^4\Sigma^-$ | $^4\Pi$ | | |
| 62 | $Co^+(3d^7 4d\ f^3D) + H$ | 13.28528 | | $^4\Pi$ | $^4\Delta$ | |
| 63 | $Co^+(3d^7 5s\ f^3H) + H$ | 13.28759 | $^4\Sigma^-$ | $^4\Pi$ | $^4\Delta$ | $^4\Phi$ |
| 64 | $Co^+(3d^7 5s\ g^3D) + H$ | 13.33463 | | $^4\Pi$ | $^4\Delta$ | |
| 65 | $Co^+(3d^7 4d\ h^3D) + H$ | 13.33582 | | $^4\Pi$ | $^4\Delta$ | |
| 66 | $Co^+(3d^7 4d\ g^3G) + H$ | 13.36719 | | $^4\Pi$ | $^4\Delta$ | $^4\Phi$ |
| 67 | $Co^+(3d^7 4d\ a^3I) + H$ | 13.36727 | | $^4\Pi$ | $^4\Delta$ | $^4\Phi$ |
| 68 | $Co^+(3d^7 4d\ g^3H) + H$ | 13.37434 | $^4\Sigma^-$ | $^4\Pi$ | $^4\Delta$ | $^4\Phi$ |
| 69 | $Co^+(3d^7 4d\ h^3F) + H$ | 13.48653 | $^4\Sigma^-$ | $^4\Pi$ | $^4\Delta$ | $^4\Phi$ |
| 70 | $Co^+(3d^7 6s\ h^5F) + H$ | 13.55333 | $^4\Sigma^-$ | $^4\Pi$ | $^4\Delta$ | $^4\Phi$ |
| 71 | $Co^+(3d^7 6s\ i^3F) + H$ | 13.60331 | $^4\Sigma^-$ | $^4\Pi$ | $^4\Delta$ | $^4\Phi$ |
| 72 | $Co^+(3d^7 4d\ i^3D) + H$ | 13.70424 | | $^4\Pi$ | $^4\Delta$ | |
| 73 | $Co^+(3d^7 5p\ w^5D^\circ) + H$ | 13.76361 | $^4\Sigma^-$ | $^4\Pi$ | $^4\Delta$ | |
| 74 | $Co^+(3d^7 5d\ i^5F) + H$ | 13.77133 | $^4\Sigma^-$ | $^4\Pi$ | $^4\Delta$ | $^4\Phi$ |
| 75 | $Co^+(3d^7 4d\ i^3P) + H$ | 13.77746 | $^4\Sigma^-$ | $^4\Pi$ | | |
| 76 | $Co^+(3d^7 4d\ j^3F) + H$ | 13.78461 | $^4\Sigma^-$ | $^4\Pi$ | $^4\Delta$ | $^4\Phi$ |
| 77 | $Co^+(3d^7 5d\ h^3G) + H$ | 13.80566 | | $^4\Pi$ | $^4\Delta$ | $^4\Phi$ |
| 78 | $Co^+(3d^7 5d\ f^5H) + H$ | 13.86608 | $^4\Sigma^-$ | $^4\Pi$ | $^4\Delta$ | $^4\Phi$ |
| 79 | $Co^+(3d^7 5p\ u^3D^\circ) + H$ | 13.86966 | $^4\Sigma^-$ | $^4\Pi$ | $^4\Delta$ | |
| 80 | $Co^+(3d^7 5d\ f^5G) + H$ | 13.87937 | | $^4\Pi$ | $^4\Delta$ | $^4\Phi$ |
| 81 | $Co^+(3d^7 5d\ h^3H) + H$ | 13.89417 | $^4\Sigma^-$ | $^4\Pi$ | $^4\Delta$ | $^4\Phi$ |
| 82 | $Co^+(3d^7 5d\ j^3D) + H$ | 13.93904 | | $^4\Pi$ | $^4\Delta$ | |
| 83 | $Co^+(3d^7 4d\ a^3K) + H$ | 14.02330 | | $^4\Pi$ | $^4\Delta$ | $^4\Phi$ |
| 84 | $Co^+(3d^7 4d\ i^3G) + H$ | 14.04457 | | $^4\Pi$ | $^4\Delta$ | $^4\Phi$ |
| 85 | $Co^+(3d^7 4d\ l^3F) + H$ | 14.06266 | $^4\Sigma^-$ | $^4\Pi$ | $^4\Delta$ | $^4\Phi$ |
| 86 | $Co^+(3d^7 5d\ j^3P) + H$ | 14.06367 | $^4\Sigma^-$ | $^4\Pi$ | | |
| 87 | $Co^+(3d^7 4d\ b^3I) + H$ | 14.12532 | | $^4\Pi$ | $^4\Delta$ | $^4\Phi$ |
| 88 | $Co^+(3d^7 4d\ k^3D) + H$ | 14.13858 | | $^4\Pi$ | $^4\Delta$ | |
| 89 | $Co^+(3d^7 4d\ i^3H) + H$ | 14.17252 | $^4\Sigma^-$ | $^4\Pi$ | $^4\Delta$ | $^4\Phi$ |
| 90 | $Co^+(3d^7 4d\ j^3G) + H$ | 14.17256 | | $^4\Pi$ | $^4\Delta$ | $^4\Phi$ |
| 91 | $Co^{2+}(3d^7\ ^4F) + H^-$ | 16.33040 | $^4\Sigma^-$ | $^4\Pi$ | $^4\Delta$ | $^4\Phi$ |

## References


1. Asplund, M. New Light on Stellar Abundance Analyses: Departures from LTE and Homogeneity. *Ann. Rev. Astron. Astrophys.* **2005**, *43*, 481. [CrossRef]
2. Barklem, P.S. Accurate abundance analysis of late-type stars: Advances in atomic physics. *Astron. Astrophys. Rev.* **2016**, *24*, 9. [CrossRef]
3. Belyaev, A.K.; Grosser, J.; Hahne, J.; Menzel, T. Ab initio cross sections for low-energy inelastic H + Na collisions. *Phys. Rev. A* **1999**, *60*, 2151–2158. [CrossRef]
4. Belyaev, A.K.; Barklem, P.S.; Dickinson, A.S.; Gadéa, F.X. Cross sections for low-energy inelastic H + Na collisions. *Phys. Rev. A* **2010**, *81*, 032706. [CrossRef]
5. Croft, H.; Dickinson, A.S.; Gadéa, F.X. A theoretical study of mutual neutralization in $Li^+ + H^-$ collisions. *J. Phys. B At. Mol. Opt. Phys.* **1999**, *32*, 81–94. [CrossRef]

6. Croft, H.; Dickinson, A.S.; Gadéa, F.X. Rate coefficients for the $Li^+/H^-$ and $Li^-/H^+$ mutual neutralization reactions. *MNRAS* **1999**, *304*, 327–329. [CrossRef]
7. Belyaev, A.K.; Barklem, P.S. Cross sections for low-energy inelastic H+Li collisions. *Phys. Rev. A* **2003**, *68*, 062703. [CrossRef]
8. Belyaev, A.K.; Barklem, P.S.; Spielfiedel, A.; Guitou, M.; Feautrier, N.; Rodionov, D.S.; Vlasov, D.V. Cross sections for low-energy inelastic Mg + H and $Mg^+ + H^-$ collisions. *Phys. Rev. A* **2012**, *85*, 032704. [CrossRef]
9. Guitou, M.; Spielfiedel, A.; Rodionov, D.S.; Yakovleva, S.A.; Belyaev, A.K.; Merle, T.; Thévenin, F.; Feautrier, N. Quantum chemistry and nuclear dynamics as diagnostic tools for stellar atmosphere modeling. *Chem. Phys.* **2015**, *462*, 94–103. [CrossRef]
10. Belyaev, A.K. Excitation cross sections in low-energy hydrogen-helium collisions. *Phys. Rev. A* **2015**, *91*, 062709. [CrossRef]
11. Mitrushchenkov, A.; Guitou, M.; Belyaev, A.K.; Yakovleva, S.A.; Spielfiedel, A.; Feautrier, N. Calcium-hydrogen interactions for collisional excitation and charge transfer. *J. Chem. Phys.* **2017**, *146*, 014304. [CrossRef]
12. Belyaev, A.K.; Vlasov, D.V.; Mitrushchenkov, A.; Feautrier, N. Quantum study of inelastic processes in low-energy calcium-hydrogen collisions. *MNRAS* **2019**, *490*, 3384–3391. [CrossRef]
13. Stenrup, M.; Larson, A.; Elander, N. Mutual neutralization in low-energy $H^+ + H^-$ collisions: A quantum ab initio study. *Phys. Rev. A* **2009**, *79*, 012713. [CrossRef]
14. Nkambule, S.M.; Elander, N.; Larson, A.; Lecointre, J.; Urbain, X.; Larson, A.; Elander, N. Differential and total cross sections of mutual neutralization in low-energy collisions of isotopes of $H^+ + H^-$. *Phys. Rev. A* **2016**, *93*, 032701. [CrossRef]
15. Drawin, H.W. Zur formelmäßigen Darstellung des Ionisierungsquerschnitts für den Atom-Atomstoß und über die Ionen-Elektronen-Rekombination im dichten Neutralgas. *Z. Phys. A Hadron. Nucl.* **1968**. [CrossRef]
16. Drawin, H.W. Validity conditions for local thermodynamic equilibrium. *Zeitschrift für Physik* **1969**, *228*, 99–119. [CrossRef]
17. Steenbock, W.; Holweger, H. Statistical equilibrium of lithium in cool stars of different metallicity. *Astron. Astrophys.* **1984**, *130*, 319–323.
18. Lambert, D.L. Quantitative stellar spectroscopy with large optical telescopes. *Phys. Scr.* **1993**, *T47*, 186–198. [CrossRef]
19. Barklem, P.S.; Belyaev, A.K.; Guitou, M.; Feautrier, N.; Gadéa, F.X.; Spielfiedel, A. On inelastic hydrogen atom collisions in stellar atmospheres. *Astron. Astrophys.* **2011**, *530*, A94. [CrossRef]
20. Thielemann, F.K.; Fröhlich, C.; Hirschi, R.; Liebendörfer, M.; Dillmann, I.; Mocelj, D.; Rauscher, T.; Martinez-Pinedo, G.; Langanke, K.; Farouqi, K.; et al. Production of intermediate-mass and heavy nuclei. *Prog. Particle Nucl. Phys.* **2007**, *59*, 74–93. [CrossRef]
21. Bergemann, M.; Pickering, J.C.; Gehren, T. NLTE analysis of CoI/CoII lines in spectra of cool stars with new laboratory hyperfine splitting constants. *MNRAS* **2010**, *401*, 1334–1346.
22. Battistini, C.; Bensby, T. The origin and evolution of the odd-Z iron-peak elements Sc, V, Mn, and Co in the Milky Way stellar disk. *Astron. Astrophys.* **2015**, *577*, A9. [CrossRef]
23. Andrews, B.H.; Weinberg, D.H.; Schönrich, R.; Johnson, J.A. Inflow, Outflow, Yields, and Stellar Population Mixing in Chemical Evolution Models. *Astrophys. J.* **2017**, *835*, 224. [CrossRef]
24. Côté, B.; O'Shea, B.W.; Ritter, C.; Herwig, F.; Venn, K.A. The Impact of Modeling Assumptions in Galactic Chemical Evolution Models. *Astrophys. J.* **2017**, *835*, 128. [CrossRef]
25. Lomaeva, M.; Jönsson, H.; Ryde, N.; Schultheis, M.; Thorsbro, B. Abundances of disk and bulge giants from high-resolution optical spectra - III. Sc, V, Cr, Mn, Co, Ni. *Astron. Astrophys.* **2019**, *625*, A141. [CrossRef]
26. Kirby, E.N.; Xie, J.L.; Guo, R.; Kovalev, M.; Bergemann, M. Catalog of Chromium, Cobalt, and Nickel Abundances in Globular Clusters and Dwarf Galaxies. *Astrophys. J. Suppl. Ser.* **2018**, *237*, 18. [CrossRef]
27. Kirby, E.N.; Xie, J.L.; Guo, R.; de los Reyes, M.A.C.; Bergemann, M.; Kovalev, M.; Shen, K.J.; Piro, A.L.; McWilliam, A. Evidence for Sub-Chandrasekhar Type Ia Supernovae from Stellar Abundances in Dwarf Galaxies. *Astrophys. J.* **2019**, *881*, 45. [CrossRef]
28. Belyaev, A.K.; Yakovleva, S.A. Estimating Inelastic Heavy-Particle-Hydrogen Collision Data. I. Simplified Model and Application to Potassium-Hydrogen Collisions. *Astron. Astrophys.* **2017**, *606*, A147. [CrossRef]

29. Belyaev, A.K.; Yakovleva, S.A. Estimating Inelastic Heavy-Particle-Hydrogen Collision Data. II. Simplified Model for Ionic Collisions and Application to Barium-Hydrogen Ionic Collisions. *Astron. Astrophys.* **2017**, *608*, A33. [CrossRef]
30. Olson, R.E.; Smith, F.T.; Bauer, E. Estimation of the Coupling Matrix Elements for One-Electron Transfer Systems. *Appl. Opt.* **1971**, *10*, 1848. [CrossRef]
31. Belyaev, A.K. Model approach for low-energy inelastic atomic collisions and application to Al + H and $Al^+ + H^-$. *Phys. Rev. A* **2013**, *88*, 052704. [CrossRef]
32. Landau, L. Zur Theorie der Energieübertragung bei Stroessen. *Phys. Z. Sowietunion* **1932**, *1*, 88–98.
33. Landau, L. Zur Theorie der Energieübertragung bei Stroessen. II. *Phys. Z. Sowietunion* **1932**, *2*, 46–51.
34. Zener, C. Non-Adiabatic Crossing of Energy Levels. *Proc. Roy. Soc. A* **1932**, *137*, 696–702. [CrossRef]
35. Belyaev, A.K.; Lebedev, O.V. Nonadiabatic nuclear dynamics of atomic collisions based on branching classical trajectories. *Phys. Rev. A* **2011**, *84*, 014701. [CrossRef]
36. Yakovleva, S.A.; Belyaev, A.K.; Kraemer, W.P. Inelastic processes in low-energy iron-hydrogen collisions. *Chem. Phys.* **2018**, *515*, 369–374. [CrossRef]
37. Yakovleva, S.A.; Belyaev, A.K.; Kraemer, W.P. Inelastic processes in low-energy collisions of singly ionized iron with hydrogen atoms. *MNRAS* **2019**, *483*, 5105–5109. [CrossRef]
38. Barklem, P.S.; Belyaev, A.K.; Asplund, M. Inelastic H + Li and $H^-$ + $Li^+$ collisions and non-LTE Li I line formation in stellar atmospheres. *Astron. Astrophys.* **2003**, *409*, L1–L4. [CrossRef]
39. Lind, K.; Asplund, M.; Barklem, P.S.; Belyaev, A.K. Non-LTE Calculations for Neutral Na in Late-Type Stars Using Improved Atomic Data. *Astron. Astrophys.* **2011**, *528*, A103. [CrossRef]
40. Mashonkina, L.; Sitnova, T.; Belyaev, A.K. Influence of Inelastic Collisions with Hydrogen Atoms on the Non-LTE Modelling of Ca I and Ca II Lines in Late-Type Stars. *Astron. Astrophys.* **2017**, *605*, A53. [CrossRef]
41. Belyaev, A.K.; Voronov, Y.V. Inelastic Processes in Low-energy Sulfur–Hydrogen Collisions. *Astrophys. J.* **2020**, *893*, 59. [CrossRef]
42. Domcke, W. Theory of resonance and threshold effects in electron-molecule collisions: The projection-operator approach. *Phys. Rep.* **1991**, *208*, 97. [CrossRef]
43. Grupp, F. MAFAGS-OS: New opacity sampling model atmospheres for A, F and G stars. I. The model and the solar flux. *Astron. Astrophys.* **2004**, *420*, 289–305. [CrossRef]
44. Grupp, F. MAFAGS-OS: New opacity sampling model atmospheres for A, F and G stars. II. Temperature determination and three "standard" stars.*Astron. Astrophys.* **2004**, *426*, 309–322. [CrossRef]
45. Butler, K.; Giddings, J. *Newsletter on Analysis of Astronomical Spectra No. 9*; University College London: London, UK, 1985.
46. Reetz, J. Sauerstoff in Kühlen Sternen und die Chemische Entwicklung der Galaxis. Ph.D. Thesis, LMU, München, Germany, 1999.
47. Belyaev, A.K.; Voronov, Y.V.; Yakovleva, S.A. Inelastic processes in calcium-hydrogen ionic collisions with account for fine structure. *Phys. Rev. A* **2019**, *100*, 062710. [CrossRef]
48. Kramida, A.; Ralchenko, Y.; Reader, J.; NIST ASD Team. NIST Atomic Spectra Database (Version 5.7.1). Available online: http://physics.nist.gov/asd (accessed on 18 October 2019).


**Sample Availability:** The calculated rate coefficients are available from the authors.